 CMC, vol.16, no.1, pp.75-100, 2010

Evaluation of the Toupin-Mindlin Theory for Predicting the Size Effects in the Buckling of the Carbon Nanotubes

Veturia Chiroiu[1], **Ligia Munteanu**[1] **and Pier Paolo Delsanto**[2]

Abstract: Conventional continuum theories are unable to capture the observed indentation size effects, due to the lack of intrinsic length scales that represent the measures of nanostructure in the constitutive relations. In order to overcome this deficiency, the Toupin-Mindlin strain gradient theory of nanoindentation is formulated in this paper and the size dependence of the hardness with respect to the depth and the radius of the indenter for multiple walled carbon nanotubes is investigated. Results show a peculiar size influence on the hardness, which is explained via the shear resistance between the neighboring walls during the buckling of the multi-walled nanotubes.

Keywords: Toupin-Mindlin strain gradient theory, nanoindentation, size effects, buckling, carbon nanotubes.

1 Introduction

Nanoindentation is a testing method which received considerable recent interest in the mechanical characterization of materials [Tabor (1951); Johnson (1985); Oliver and Pharr (1992); Collin *et al.* (2008); Dumitriu and Chiroiu (2006, 2008); Dumitriu *et al*. (2008); Misra and Huang (2009; Keerthika *et al.* (2009)]. The goal of such testing is to extract elastic modulus and hardness of the specimen material from readings of indenter load and depth of penetration [Qian *et al*. (2008)]. The forces involved are usually of the order of mN (1mN = 10^{-3}N) range and are measured with a resolution of the order of nN (1nN =10^{-9}N). The depths of penetration are of the order of microns with a resolution of less than a nanometre (10^{-9}N).

The size dependence of the nanoindentation is an open problem. There are numerous indentation tests at scales on the order of a micron or a submicron which have shown that the hardness increases significantly with decreasing the indenter

[1] Institute of Solid Mechanics of Romanian Academy, Ctin Mille 15, 010141 Bucharest
[2] Politecnico of Torino, Physics Department, Corso Duca degli Abruzzi 24, 10129 Torino

size [Abu (2007)]. This can be attributed to the evolution of the so-called geometrically necessary dislocations beneath the indenter, which gives rise to strain gradients. On the micron or nanometer scale, the size effect of the deformation is inherent [Hutchinson (2000); Evans and Hutchinson 2009]. Similarly indentation on the nano/microscale also displays a strong size effect. For example, the spreading of intershell distances and the inlayer van der Waals interactions in carbon nanotubes depend on the size of the tube [Brenner *et al*. (2002); Srivastava and Atluri (2002); Nair *et al*. (2008); Cheng *et al.* (2009)]. We add the dependency on the size of the tube of the dispersive characteristics, group velocities of multiwalled carbon nanotubes [Xie *et al.* (2007)].The mechanical properties are size dependent with respect to different dimensions and geometries of the carbon nanotubes [Theodosiou and Saravanos (2007); Chen *et al*. (2007); Solano *et al.* (2008); Chiroiu *et al*. (2006): Munteanu and Chiroiu (2009); Jeng *et al.* (2009); Giannopoulos *et al*. (2010)]. The indentation hardness of metals and ceramics increases with respect to decreasing the indenter size below 10 micron-size indents [Ma and Clarke (1995); Poole *et al*. (1996); Begley and Hutchinson (1998)].

The necessity for higher-order continuum theories originates from the inability of the classical theories to account for observed the size effects on the micro and nanoscales [Toupin (1962); Mindlin (1964)]. These effects usually manifest themselves as an increase in the strength with respect to decreasing the size of the structure when the length scale is of the order of microns.

Principal methods of the theoretic study on carbon nanotubes are atomistic simulation, continuum model and multi-scale simulation methods. Atomistic techniques are defective for simulation of phenomena occurring on a vast range of length scales. So far, a few continuum mechanics methods have been adopted for studying the carbon nanotubes [Ru (2001); Li and Chou (2003); Nasdala *et al.* (2005)]. Multi-scale simulation methods in nanomechanics are used by Gumbsch (1996); Hiroshi Kadowaki and Wing Kam Liu (2005) and Shen and Atluri (2004). The results obtained by Xie and Long (2006) show that micropolar theory which takes into account the microdeformation, can also be employed to analyze the mechanics behaviors of nanostructure. The micropolar mechanics demand the fewer elements than the molecular structural mechanics, and its computational time is shorter than the molecular structural mechanics. Computational homogenisation can be also used to couple two different continuum at macro scale, classical and gradient [Kaczmarczyk {2006)].

The necessity for higher-order continuum theories originates from the inability of the classical theories to account for observed the size effects on the micro and nanoscales [Toupin (1962); Mindlin (1964)]. These effects usually manifest themselves as an increase in the strength with respect to decreasing the size of the struc-

ture when the length scale is of the order of microns.

The lack of intrinsic length scales that represent the measures of microstructure in their constitutive relations in conventional continuum theories is very well known [Kikuchi *et al.* (1985): Fleck and Hutchinson (1993, 1997, 2001); Chambon *et al*. (1996, 1998, 2001, 2004); Georgiadis *et al*. (2000); Kaczmarczyk (2005); Georgiadis and Grentzelou (2006); Zhao *et al*., 2005, 2006, 2007a,b; Zhao and Sheng (2006)]. The importance of a potential function relies on simplification of the quantum mechanics and ab initio complexity. These simplifications are very important once it can provide analytical solutions of materials properties [Chakrabarty and Cagin (2008); Rino *et al* (2009)]. The multiscale nonlinear tensorial constitutive modeling of carbon nanostructures is based on the interatomic potentials. Using a constitutive model written as a tensorial equation relating the second Piola-Kirchhoff stress tensor to Green-Lagrange strain tensor, the elastic behavior of the graphene sheet and carbon nanotube are studied by Ghanbari and Naghdabadi (2009).

Some new and recent results for 3D solid mechanics problems involving the strain-gradient theories of material inelasticity are obtained by Tang, Shen and Atluri (2003). The novel use of the Meshless Local Petrov Galerkin Method (MLPG) is generating a variety of meshless methods and algorithms for molecular dynamics, and for multiple-length&-time scale simulations [Atluri and Zhu (1998); Atluri and Shen (2002 a,b); Han and Atluri (2003); Atluri, Han and Shen (2003): Li *et al*. (2003)].

In parallel with Mindlin's (1965) second-order strain gradient theory (or grade-three elasticity), the Toupin-Mindlin theory which is sometimes also called the first strain gradient theory in elasticity or the linear theory of solids of grade two [Toupin (1964); Mindlin and Eshel (1968); Eshel and Rosenfeld (1970, 1975)], where the term grade indicates the order of the space gradients operating on the displacement.

The original Toupin–Mindlin strain gradient theory has been formulated in general tensor forms. The general formulations of this theory for the cases of cylindrical coordinates and spherical coordinates are derived by Zhao and Pedroso in 2008, following the approach and notation used by Eringen (1967) for the translation of conventional elasticity theories from rectangular coordinates to orthogonal curvilinear coordinates.

In the viscoeplasticity range, a strain-gradient theory for isotropic viscoplastic materials was also proposed [Lele and Anand (2009)]. Lele and Anand have applied their gradient viscoplasticity theory to simulate the size-effect regarding hardness versus the indentation depth in nano/micro-indentation experiments.

Very few experimental results exist for the shell buckling of nanotubes. A remark-

able work in this direction is due to Waters *et al*. (2005). They measured the critical shell-buckling load by an experimental technique in which individual multiwalled carbon nanotubes are axially compressed using a nanoindenter.

The objective of this paper is to investigate the size dependence of the hardness with respect to the depth and the indenter radius for the shell buckling of multiwalled carbon nanotubes. The Toupin-Mindlin strain gradient theory is used to explain the size influence on the hardness, by taking account on the higher-order stress gradient contribution in the shear resistance of the neighboring walls during buckling of the multiwalled nanotubes.

2 Toupin-Mindlin strain gradient theory of nanoindentation

The indentation test consists of measuring simultaneously the indentation load P and indentation depth h during the normal penetration of an indenter into a sample of volume V and surface$S$. The scheme of the indentation with a flat-ended cylindrical punch, a conical indenter with the apex angle2α, and a spherical indenter with a diameter $2R$ are shown in Figs.1(a)-(c), respectively. The in-plane dimensions and the thickness of the indented material, normal to the indented surface, are much larger than the diameter $2a$ of the largest imprint made on it by the indenter. In the rectangular coordinate system, the in-plane is denoted by(x,y) and the radial direction is denoted by$r$, while the out-of-plane direction is denoted by$z$. At the indented surface we have $z=0$. The process modeled here represents quasi-static, frictionless, normal indentation of a transversely isotropic material by an axisymmetric rigid indenter.

The hardness H is given by the following relationship, where A is the contact area

$$H=\frac{P}{A} \tag{2.1}$$

Many studies have been elaborated in order to determine the contact area [Hernot *et al*. (2006); Li *et al*. (1997)]. Hill *et al.* (1989)] have introduced a factor C^2 to quantify the degree of piling-up ($C^2>1$) or sinking-in ($C^2<1$) during the indentation test. Li *et al*. (1997) suggested the determination of a relationship between the indentation load P and depth h in the elastic regime using the results deduced from the Hertz elastic

$$P=\frac{4}{3}\frac{E}{1-\nu^2}h\sqrt{hR}, \tag{2.2}$$

where E is the Young's modulus and ν is the Poisson ratio. In the Hertz theory, the contact radius a is $\sqrt{Rh}$ and therefore Eq. (2.2) becomes

$$P=\frac{4}{3}\frac{Eah}{1-\nu^2}. \tag{2.3}$$

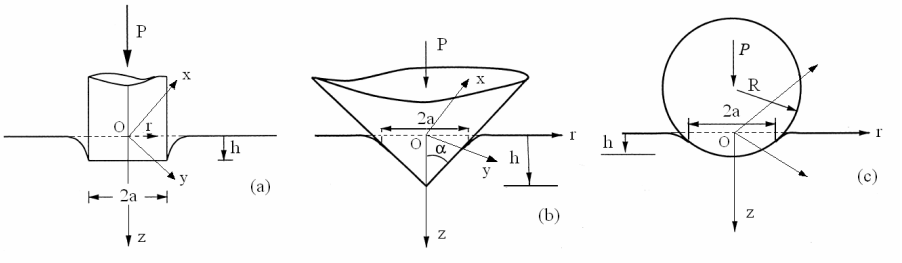

Figure 1: Scheme of the indentation with a flat-ended cylindrical punch (a), a conical indenter (b) and a spherical indenter (c).

The initial unloading stiffness for every kind of axisymmetric indenters, can be defined as follows [Galin (1946); Sneddon (1965); Bulychev *et al.* (1975, 1976); Shorshorov *et al.* (1981); Wolff (2001)]

Now, let us consider a gradient-dependent material body with volume V and surface S, which is normally indented by an axisymmetric indenter.

Let us consider the Toupin-Mindlin strain gradient theory in the rectangular coordinate system. We assume that the strain gradient tensor η_{ijk} and the double stress tensor τ_{ijk} with dimensions force per unit length, are present in the material body together with the conventional Eulerian strain tensor ε_{ij} and Cauchy stress tensor σ_{ij}. The components of the strain and strain gradient tensors are defined by

$$\varepsilon_{ij} = \frac{1}{2}(u_{i,j} + u_{j,i}), \quad \eta_{ijk} = \varepsilon_{jk,i} = u_{k,ij} = \eta_{ikj}, \quad i,j,k = 1,2,3, \tag{2.4}$$

where u_i, $i = 1,2,3$ are displacements. ε_{ij} and η_{ijk} are symmetric with respect to the indices i and j, and accordingly, the Cauchy stress tensor σ_{ij} and the double stress tensor τ_{ijk} are also symmetric with respect to i and j. Consequently, under any small perturbations of the strains and strain gradients, $\delta\varepsilon_{ij}$ and $\delta\eta_{ijk}$, the work deviation may be obtained by the two pairs of work-conjugates

$$\delta W = \sigma_{ij}\delta\varepsilon_{ij} + \tau_{ijk}\delta\eta_{ijk}.$$

In addition, within the framework of linear elasticity, the following generalized Hooke's law between σ_{ij} and ε_{ij}, and τ_{ijk} and η_{ijk}, respectively, is assumed

$$\sigma_{ij} = \lambda\varepsilon_{kk}\delta_{ij} + 2\mu\varepsilon_{ij},$$

$$\begin{aligned}\tau_{ijk} =&\xi_1 l^2(\eta_{ipp}\delta_{jk}+\eta_{jpp}\delta_{ik})+\xi_2 l^2(\eta_{ppi}\delta_{jk}+2\eta_{kpp}\delta_{ij}+\eta_{ppj}\delta_{ik})+\\ &+\xi_3 l^2\eta_{ppk}\delta_{ij}+\xi_4 l^2\eta_{ijk}+\xi_5 l^2(\eta_{kji}+\eta_{kij}),\end{aligned} \tag{2.5}$$

where λ and μ are the conventional Lamé constants, ξ_i, $i=1,2,...,5$, are the elastic constants associated with the gradient terms, while l denotes an internal length scale resulted by the introduction of the strain gradients. It is related to the dimension of microstructure in the material. The positive definiteness of the strain energy density requires

$$\mu>0,\quad 3\lambda+2\mu>0,\quad \bar{\xi}_2>0,\quad 5\bar{\xi}_1+2\bar{\xi}_2>0,$$

$$-\bar{d}_1<\bar{d}_2<\bar{d}_1,\quad 5\bar{f}^2<6(\bar{d}_1-\bar{d}_2)(5\bar{\xi}_1+2\bar{\xi}_2),$$

$$18\bar{d}_1=-2\xi_1+4\xi_2+\xi_3+6\xi_4-3\xi_5,$$

$$18\bar{d}_2=2\xi_1-4\xi_2-\xi_3,\quad 3\bar{\xi}_1=2(\xi_1+\xi_2+\xi_3),$$

$$\bar{\xi}_2=\xi_4+\xi_5,\quad 3\bar{f}=\xi_1+4\xi_2-2\xi_3.$$

In the absence of body and inertia forces, the equilibrium equations written in terms of Cauchy stress σ_{ij} and the higher-order stress τ_{ijk} are

$$\sigma_{ik,i}-\tau_{ijk,ji}=0. \tag{2.6}$$

Substituting Eqs. (2.4) and (2.5) into Eq. (2.6), the equilibrium equations can be written with respect to displacements

$$\begin{aligned}&\lambda u_{p,pi}\delta_{ik}+\mu(u_{i,ki}+u_{k,ii})-\xi_1 l^2(u_{p,ipji}\delta_{jk}+u_{p,jpji}\delta_{ik})-\\ &-\xi_2 l^2(u_{i,ppji}\delta_{jk}+2u_{p,kpji}\delta_{ij}+u_{j,ppji}\delta_{ik})-\xi_3 l^2 u_{k,ppji}\delta_{ij}-\\ &-\xi_4 l^2 u_{k,ijji}-\xi_5 l^2(u_{i,kjji}+u_{j,kiji})=0,\end{aligned} \tag{2.7}$$

To write the boundary conditions, the external surface S may be divided into two parts: the surface boundary S_σ for static forces, and the surface boundary S_u for displacements. On S_σ, the boundary conditions read as

$$T_k=n_i(\sigma_{ik}-\partial_j\tau_{ijk}),\quad R_k=n_i n_j\tau_{ijk},$$

where T_k and R_k are the surface tractions and higher-order surface tractions, respectively. The above boundary conditions represent the conventional traction and higher-order traction conditions for a gradient-dependent material body. In the following we suppose that the contribution of τ_{ijk} is zero. So, T_k and R_k become

$$T_k=n_i\sigma_{ik},\quad R_k=0. \tag{2.8}$$

On S_u the boundary conditions are given by

$$u_k = \bar{u}_k, \quad n_l \partial_l u_k = \bar{e}_k, \tag{2.9}$$

where $\bar{u}_k$ denotes the known displacements and $\bar{e}_k$ represent the known normal gradient of $\bar{u}_k$. A rigorous derivation of the kinematic conditions in Eq.(2.9b) was given by Georgiadis and Grentzelou (2006) using the principle of complementary virtual work and a Hellinger–Reissner-type variational principle.

2.1 Spherical nanoindentation

In order to study the buckling of multiple walled carbon nanotubes, the spherical indentation is used. In conjunction with the strain gradient theory of nanoindentation, the spherical coordinate description is necessary. The in-plane radial direction is denoted by r, the in-plane angular position is denoted by θ, while the out-of-plane angular position is denoted by φ. The indenter is a rigid sphere of radius R as shown in Fig. 1c. The indenter is loaded with a normal force$P$, and the hardness H is given by Eq. (2.1).

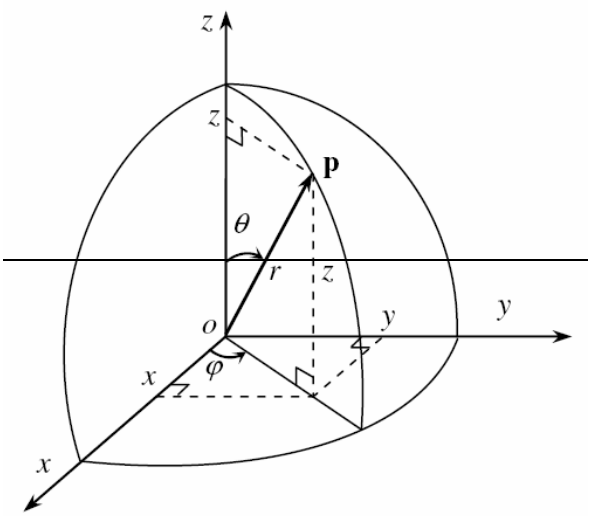

Figure 2: Spherical coordinates

The spherical coordinates (r, θ, φ) are related to the rectangular coordinates (x, y, z) by (see also Fig. 2)

$$x = r\sin\theta\cos\varphi, \quad y = r\sin\theta\sin\varphi, \quad z = r\cos\theta.$$

In the absence of body forces, the gradient-dependent equilibrium equations (2.6), written in spherical coordinates are given by [Volokh (2006); Zhao and Pedroso (2008)]

$$\begin{aligned}
&\sigma^*_{rr,r}+\frac{1}{r}\sigma^*_{\theta r,\theta}+\frac{1}{r\sin\theta}\sigma^*_{\varphi r,\varphi}+\frac{1}{r}(2\sigma^*_{rr}-\sigma^*_{\theta\theta}-\sigma^*_{\varphi\varphi}+\sigma^*_{\theta r}\cot\theta)=0,\\
&\sigma^*_{r\theta,r}+\frac{1}{r}\sigma^*_{\theta\theta,\theta}+\frac{1}{r\sin\theta}\sigma^*_{\varphi\theta,\varphi}+\frac{1}{r}(2\sigma^*_{r\theta}+\sigma^*_{\theta r}+(\sigma^*_{\theta\theta}+\sigma^*_{\varphi\varphi})\cot\theta)=0,\\
&\sigma^*_{r\varphi,r}+\frac{1}{r}\sigma^*_{\theta\varphi,\theta}+\frac{1}{r\sin\theta}\sigma^*_{\varphi\varphi,\varphi}+\frac{1}{r}(2\sigma^*_{r\varphi}+\sigma^*_{\varphi r}+2\sigma^*_{\varphi\theta}\cot\theta)=0.
\end{aligned} \tag{2.10}$$

where σ^*_{ij} is the generalized stress components given by

$$\begin{aligned}
\sigma^*_{rr}=\sigma_{rr}-(&\tau_{rrr,r}+r^{-1}\tau_{r\theta r,\theta}+r^{-1}\tau_{r\varphi r,\varphi}\sin^{-1}\theta\\
&+r^{-1}(2\tau_{rrr}-\tau_{\theta\theta r}-\tau_{r\theta\theta}-\tau_{\varphi\varphi r}-\tau_{r\varphi\varphi}+\tau_{r\theta r}\cot\theta)),
\end{aligned}$$

$$\begin{aligned}
\sigma^*_{\theta r}=\sigma_{\theta r}--(&\tau_{\theta rr,r}+r^{-1}\tau_{\theta\theta r,\theta}+r^{-1}\tau_{\theta\varphi r,\varphi}\sin^{-1}\theta\\
&+r^{-1}(2\tau_{\theta rr}+\tau_{r\theta r}-\tau_{\theta\theta\theta}-\tau_{\theta\varphi\varphi}-\tau_{r\varphi\varphi}+(\tau_{\theta\theta r}-\tau_{\varphi\varphi r})\cot\theta)),
\end{aligned}$$

$$\begin{aligned}
\sigma^*_{\varphi r}=\sigma_{\varphi r}-(&\tau_{\varphi rr,r}+r^{-1}\tau_{\varphi\theta r,\theta}+r^{-1}\tau_{\varphi\varphi r,\varphi}\sin^{-1}\theta\\
&+r^{-1}(3\tau_{\varphi rr}-\tau_{\varphi\theta\theta}-\tau_{\varphi\varphi\varphi}+2\tau_{\varphi\theta r}\cot\theta)),
\end{aligned}$$

$$\begin{aligned}
\sigma^*_{\theta\theta}=\sigma_{\theta\theta}-(&\tau_{\theta r\theta,r}+r^{-1}\tau_{\theta\theta\theta,\theta}+r^{-1}\tau_{\theta\varphi\theta,\varphi}\sin^{-1}\theta\\
&+r^{-1}(3\tau_{r\theta\theta}+\tau_{\theta\theta r}+(\tau_{\theta\theta\theta}-\tau_{\varphi\varphi\theta}-\tau_{\theta\varphi\varphi})\cot\theta)),
\end{aligned}$$

$$\begin{aligned}
\sigma^*_{r\theta}=\sigma_{r\theta}--(&\tau_{rr\theta,r}+r^{-1}\tau_{r\theta\theta,\theta}+r^{-1}\tau_{r\varphi\theta,\varphi}\sin^{-1}\theta\\
&+r^{-1}(2\tau_{rr\theta}+\tau_{r\theta r}-\tau_{\theta\theta\theta}-\tau_{\varphi\varphi\theta}-\tau_{r\varphi\varphi}+(\tau_{r\theta\theta}-\tau_{r\varphi\varphi})\cot\theta)),
\end{aligned} \tag{2.11}$$

$$\begin{aligned}
\sigma^*_{\varphi\theta}=\sigma_{\varphi\theta}--(&\tau_{\varphi r\theta,r}+r^{-1}\tau_{\varphi\theta\theta,\theta}+r^{-1}\tau_{\varphi\varphi\theta,\varphi}\sin^{-1}\theta\\
&+r^{-1}(3\tau_{r\varphi\theta}+\tau_{\varphi\theta r}+(\tau_{\theta\varphi\theta}+\tau_{\varphi\theta\theta}-\tau_{\varphi\varphi\varphi})\cot\theta)),
\end{aligned}$$

$$\begin{aligned}
\sigma^*_{\varphi\varphi}=\sigma_{\varphi\varphi}-(&\tau_{\varphi r\varphi,r}+r^{-1}\tau_{\varphi\theta\varphi,\theta}+r^{-1}\tau_{\varphi\varphi\varphi,\varphi}\sin^{-1}\theta\\
&+r^{-1}(3\tau_{r\varphi\varphi}+\tau_{\varphi\varphi r}+(2\tau_{\theta\varphi\varphi}+\tau_{\varphi\varphi\theta})\cot\theta)),
\end{aligned}$$

$$\sigma^*_{r\varphi} = \sigma_{r\varphi} - -(\tau_{rr\varphi,r} + r^{-1}\tau_{r\theta\varphi,\theta} + r^{-1}\tau_{r\varphi\varphi,\varphi}\sin^{-1}\theta + r^{-1}(2\tau_{rr\varphi} + \tau_{r\varphi r} - \tau_{\theta\theta\varphi} - \tau_{\varphi\varphi\varphi} + (\tau_{r\theta\varphi} + \tau_{r\varphi\theta})\cot\theta)),$$

$$\sigma^*_{\theta\varphi} = \sigma_{\theta\varphi} - (\tau_{\theta r\varphi,r} + r^{-1}\tau_{\theta\theta\varphi,\theta} + r^{-1}\tau_{\theta\varphi\varphi,\varphi}\sin^{-1}\theta + r^{-1}(3\tau_{r\theta\varphi} + \tau_{\theta\varphi r} + (\tau_{\theta\varphi\theta} + \tau_{\theta\theta\varphi} - \tau_{\varphi\varphi\varphi})\cot\theta))$$

The physical components for strains are given by

$$\varepsilon_{rr} = u_{r,r}, \quad \varepsilon_{\theta\theta} = r^{-1}(u_{\theta,r} + u_r), \quad \varepsilon_{\varphi\varphi} = r^{-1}(u_{\varphi,\varphi}\sin^{-1}\theta + u_r + u_\theta\cot\theta),$$
$$2\varepsilon_{r\varphi} = 2\varepsilon_{\varphi r} = r^{-1}(u_{r,\varphi}\sin^{-1}\theta + u_{\varphi,r} - u_\varphi), \tag{2.12}$$
$$2\varepsilon_{\theta\varphi} = 2\varepsilon_{\varphi\theta} = r^{-1}(u_{\varphi,\theta} + u_{\theta,\varphi}\sin^{-1}\theta - u_\varphi\cot\theta).$$

The physical components for strain gradients in spherical coordinates are given by

$$\eta_{rrr} = u_{r,rr}, \quad \eta_{\theta\theta r} = r^{-2}(u_{r,\theta\theta} + ru_{r,r} - 2u_{\theta,\theta} - u_r),$$

$$\eta_{\varphi\varphi r} = r^{-2}u_{r,\varphi\varphi}\sin^{-2}\theta + r^{-1}u_{r,r} + r^{-2}u_{r,\theta}\cot\theta - 2r^{-2}u_{\varphi,\varphi}\sin^{-1}\theta - r^{-2}u_r - 2r^{-2}u_\theta\cot\theta),$$

$$\eta_{\theta rr} = \eta_{r\theta r} = r^{-1}(u_{r,r\varphi} - r^{-1}u_{r,\theta} - u_{\theta,r} + 3r^{-1}u_\theta),$$
$$\eta_{\varphi rr} = \eta_{r\varphi r} = r^{-1}\sin^{-1}\theta(u_{r,r\varphi} - r^{-1}u_{r,\varphi} - u_{\varphi,r}\sin\theta + 1.5r^{-1}u_\varphi\sin^{-1}\theta),$$
$$\eta_{\varphi\theta r} = \eta_{\theta\varphi r} = r^{-2}\sin^{-1}\theta(u_{r,\theta\varphi} - u_{r,\varphi}\cot\theta - u_{\varphi,r}\sin\theta - u_{\theta,\varphi} + 2u_\varphi\cos\theta),$$
$$\eta_{rr\theta} = u_{\theta,rr} + r^{-2}u_\theta, \quad \eta_{\theta\theta\theta} = r^{-1}(r^{-1}u_{\theta,\theta\theta} + 2r^{-1}u_{r,\theta} + u_{\theta,r} - r^{-1}u_\theta), \tag{2.13}$$

$$\eta_{\varphi\varphi\theta} = r^{-2}u_{\theta,\varphi\varphi}\sin^{-2}\theta - r^{-2}u_{\varphi,\varphi}\cot\theta\sin^{-1}\theta + r^{-2}u_{\theta,\theta}\cot\theta + r^{-1}u_{\theta,r} - r^{-2}u_\theta\cot^2\theta),$$

$$\eta_{\theta r\theta} = \eta_{r\theta\theta} = r^{-1}(u_{\theta,r\theta} + u_{r,r} - r^{-1}u_{\theta,\theta} - 0.5r^{-1}u_r),$$
$$\eta_{\varphi r\theta} = \eta_{r\varphi\theta} = r^{-1}\sin^{-1}\theta(u_{\theta,r\varphi} - r^{-1}u_{\theta,\varphi} - (u_{\varphi,r} - 0.5r^1u_\varphi)\cos\theta),$$

$$\eta_{\varphi\theta\theta} = \eta_{\theta\varphi\theta} = r^{-2}\sin^{-1}\theta(u_{\theta,\theta\varphi} + u_{r,\varphi} - u_{\theta,\varphi}\cot\theta - u_{\varphi,\theta}\cos\theta + 0.5u_\varphi(3\cot\theta\cos\theta - \sin\theta),$$

$$\eta_{rr\varphi} = u_{\varphi,rr}, \quad \eta_{\theta\theta\varphi} = r^{-1}(r^{-1}u_{\varphi,\theta\theta} + u_{\varphi,r} + r^{-1}u_\phi\sin^{-2}\theta),$$

$$\eta_{\varphi\varphi\varphi} = r^{-1}\sin^{-1}\theta(r^{-1}u_{\varphi,\varphi\varphi}\sin^{-1}\theta + 2r^{-1}u_{r,\varphi} + 2r^{-1}u_{\theta,\varphi}\cot\theta + u_{\varphi,r}\sin\theta + + r^{-1}u_{\varphi,\theta}\cos\theta - r^{-1}u_{\varphi}\sin^{-1}\theta),$$

$$\eta_{\theta r\varphi} = \eta_{r\theta\varphi} = r^{-1}(u_{\varphi,r\theta}\sin^{-1}\theta - r^{-1}u_{\varphi,\theta}),$$

$$\eta_{\varphi r\varphi} = \eta_{r\varphi\varphi} = r^{-1}(u_{\varphi,r\varphi}\sin^{-1}\theta - r^{-1}u_{\varphi,\varphi}\sin^{-1}\theta + u_{r,r} + (u_{\theta,r} - r^{-1}u_{\theta})\cot\theta - 0.5r^{-1}u_r).$$

$$\eta_{\varphi\theta\varphi} = \eta_{\theta\varphi\varphi} = r^{-2}(u_{\varphi,\theta\varphi}\sin^{-1}\theta - u_{r,\varphi}\sin^{-1}\theta\cot\theta + u_{r,\theta} + u_{\theta,\theta}\cot\theta - 0.5u_{\theta}\sin^{-2}\theta).$$

The boundary conditions (2.8) and (2.9) become

$$T_r = n_p\sigma^*_{pr}, \quad T_\theta = n_p\sigma^*_{p\theta}, \quad T_\varphi = n_p\sigma^*_{p\varphi}, \tag{2.14}$$

on S_σ, and

$$u_r = \bar{u}_r, \quad u_\theta = \bar{u}_\theta, \quad u_\varphi = \bar{u}_\varphi, \tag{2.15}$$

$$n_r u_{r,r} + rn_\theta(u_{r,\theta} - u_\theta) + rn_\varphi\sin\theta(u_{r,\varphi} - u_\varphi\sin\theta) = \bar{e}_r,$$

$$n_r u_{\theta,r} + rn_\theta(u_{\theta,\theta} + u_r) + rn_\varphi\sin\theta(u_{\theta,\varphi} - u_\varphi\cos\theta) = \bar{e}_\vartheta,$$

$$n_r u_{\varphi,r} + rn_\theta u_{\varphi,\theta} + rn_\varphi\sin\theta(u_{\varphi,\varphi} + u_r\sin\theta + u_\theta\cos\theta) = \bar{e}_\varphi,$$

on S_u.

2.2 Nanoindentation simulation

The aim of this study is to simulate the nanoindentation test for multiple walled carbon nanotubes inspired from the papers of Munteanu and Chiroiu (2009) and Waters *et al.* (2005). Waters *et al*. (2005) have used a 10μm radius sphere indenting the nanotubes, with an extremely fine force and displacement resolution ($\approx$300nm and $\approx$1 nm, respectively).

In our paper we consider the axially compressed multiple walled carbon nanotube (MWCN) of diameter d =50nm, and length L =100nm, by a nanoindentation technique. The nanotubes used in our study have 15 walls with an interwall spacing of 0.34nm, the outer radius is R_{outer} =25 nm, and the inner radius is R_{inner} =20 nm.

In order to study the buckling of multiple walled carbon nanotubes, different radii of the spherical indenter are considered. The indenting surface is practically flat and all the nanotubes located near the center of the indent undergo shell buckling.

The contact area used in the calculation is very closed to the cross-sectional area of the MWCN [Li and Chou 2003]

$$A = \pi\alpha[(R_{outer} + 0.17)^2 - (R_{inner} - 0.17)^2], \tag{2.16}$$

where $0 \leq \alpha \leq 1$ and the half layered thickness of the nanotube is 0.17. The scheme of the indentation of carbon nanotubes and shell buckling is presented in Fig.3.

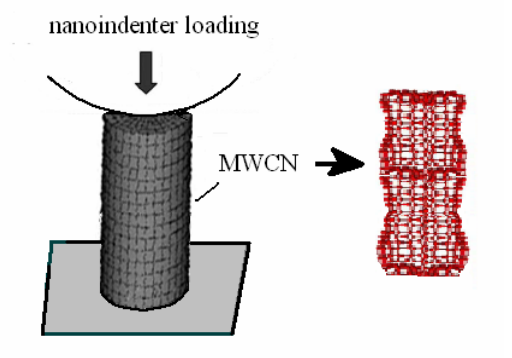

Figure 3: Scheme of the indentation and shell buckling

The load-unloaded-displacement curve is presented in Fig.4. This curve was theoretically obtained by Munteanu and Chiroiu (2009), by applying a method that combines the features of nonlocal theory and molecular mechanics. The deformation of compressed multiple walled carbon nanotubes was investigated, with the emphasis on the simulation of the nanoindentation technique in order to compare the proposed method to available experimental results. The performance of the method was carefully verified by numerical experiments. The theoretical results obtained by Munteanu and Chiroiu (2009) were found to be in very good agreement with the experimental data reported by Waters, Gudury, Jouzi and Xu (2005).

In Fig. 4, as the experiments report, the loading portion consists of three stages: an initial linear increase, then a sudden drop in the slope with the curve becoming flat, and a third stage comprising and increasing load.

The sudden decrease in the slope is the signature CNT buckling, which indicates the collapse process.

After buckling, the neighbouring nanotubes come into contact with the indenter tip, which results in an increase in the load, as can be seen from Fig. 4 in the third stage. The position of the zero displacement corresponds to a nonzero load. According to

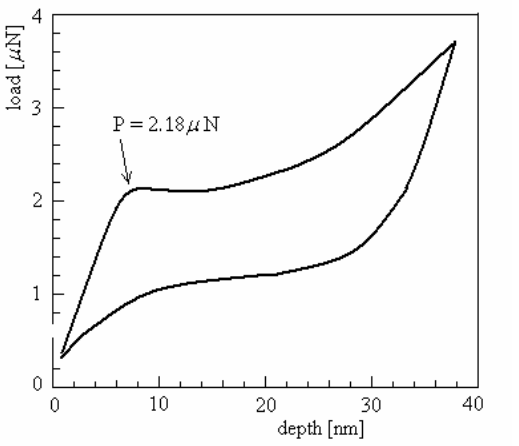

Figure 4: Scheme of the load-unloaded-displacement curve

this simulation, the critical buckling is obtained as 2.18μN, which is very close to the experimental result (in the range 2.0-2.5μN).

3 General solutions for the boundary value problem

By substituting Eqs. (2.11), (2.12) and (2.13) into Eq. (2.10), the equilibrium equations can be written with respect to the displacements u_r, u_θ and u_φ. In the displacement form, the equilibrium equations (2.10) along with the boundary conditions (2.14) and (2.15) can be analytically solved by using the cnoidal method. The equilibrium equations written with respect to a new variable $\zeta = k_r r + k_\theta \theta + k_\varphi \varphi$, with the unknown wave numbers k_r, k_θ and k_φ can be reduced to the Weierstrass equations with polynomials of higher-order, similar to

$$u_{,\zeta}^2 = \sum_{j=0}^{n} A_j(\zeta) u^j. \tag{3.1}$$

The cnoidal method was proposed by Munteanu and Donescu (2004) for solving nonlinear equations, as a further extension of the Osborne method (1995). The general solutions of the equilibrium equations can be written in the form [Munteanu and Chiroiu (2010)]

$$u_i = u_{i\text{lin}} + u_{i\text{nonlin}}, \quad i = r, \theta, \varphi, \tag{3.2}$$

where the linear and nonlinear terms express the linear and nonlinear superposition

respectively, of cnoidal functions

$$u_{\text{lin}} = 2\sum_{k=0}^{n} \alpha_k \text{cn}^2(\omega_k \zeta; m_k),$$

$$u_{\text{nonlin}} = \frac{\sum_{k=0}^{n} \beta_k \text{cn}^2(\omega_k \zeta; m_k)}{1 + \sum_{k=0}^{n} \gamma_k \text{cn}^2(\omega_k \zeta; m_k)}. \tag{3.3}$$

In Eq. (3.3), the unknown cnoidal moduli verify the condition $0 \leq m_k \leq 1$, while the unknown quantities ω_k, α_k, β_k and γ_k depend on λ, μ, ξ and l and also on the boundary conditions (2.14) and (2.15). The theta-function representation of the solutions is used for deriving Eq. (3.3) [Data and Tanaka (1976); Dubrovin, Matseev and Novikov (1976)]. The derivation is a complicated affair drawing on many beautiful results in the theory of Hill's equation and Riemann's solution of the Jacob's inversion problem. Let us introduce the following dependent-variable transformation

$$u = 2\frac{\mathrm{d}^2}{\mathrm{d}\zeta^2} \log \Theta_n(\zeta). \tag{3.4}$$

Introducing Eq. (3.4) into Eq. (3.1), the following bilinear differential equation is obtained

$$D_\zeta^2 (1 + D_\zeta^2) \Theta_n \cdot \Theta_n = 0, \tag{3.5}$$

where the operator D_ζ is defined as $D_\zeta^m a \cdot b = (\partial_\zeta - \partial'_\zeta)^m a(\zeta) b(\zeta')|_{\zeta=\zeta'}$. The function Θ_n is given in terms of an asymptotic expansion of the following type (near-identity)

$$\Theta_n = 1 + \varepsilon \Theta_n^{(1)} + \varepsilon^2 \Theta_n^{(2)} + \ldots \quad , \tag{3.6}$$

with $\Theta_n^{(1)} = \sum_{i=1}^{n} \exp(\mathrm{i}\omega_i \zeta)$. For $n = 1$ one obtains

$$\Theta_1 = 1 + \exp(\mathrm{i}\omega_1 \zeta + B_{11}),$$

$$\Theta_2 = 1 + \exp(\mathrm{i}\omega_1 \zeta + B_{11}) + \exp(\mathrm{i}\omega_2 \zeta + B_{22}) + \exp(\omega_1 + \omega_2 + B_{12}),$$

$$\begin{aligned}\Theta_3 =& 1 + \exp(i\omega_1 \zeta + B_{11}) + \exp(\mathrm{i}\omega_2 \zeta + B_{22}) + \exp(\mathrm{i}\omega_3 \zeta + B_{33}) \\ &+ \exp(\omega_1 + \omega_2 + B_{12}) + + \exp(\omega_1 + \omega_3 + B_{13}) + \exp(\omega_2 + \omega_3 \\ &+ B_{23}) + \exp(\omega_1 + \omega_2 + \omega_3 + B_{12} + B_{13} + B_{23}).\end{aligned}$$

For an arbitrary n, the following expression is obtained

$$\Theta_n = \sum_{M=0,1} \exp(\mathrm{i}\sum_{i=1}^{n} M_i\omega_i\zeta + \frac{1}{2}\sum_{i<j}^{n} B_{ij}M_iM_j), \tag{3.7}$$

where $\exp B_{ij} = \left(\frac{\omega_i-\omega_j}{\omega_i+\omega_j}\right)^2$, $\exp B_{ii} = \omega_i^2$. In Eq. (3.7) $M = [M_1, M_2]$ is the vector of integer indices (0 and 1), $\omega = [\omega_1, \omega_2, ..., \omega_n]$ is the frequency vector, and is the finite number of degrees of freedom for a particular solution. The matrix$B$ is written as a sum of a diagonal matrix and an off-diagonal matrix. The solution (3.4) can be written in the form

$$u = 2\frac{\mathrm{d}^2}{\mathrm{d}t^2}\log\Theta_n(\zeta) = 2\frac{\mathrm{d}^2}{\mathrm{d}t^2}\log G(\zeta) + 2\frac{\mathrm{d}^2}{\mathrm{d}t^2}\log\left(1+\frac{F(\zeta)}{G(\zeta)}\right),$$

$$G(t) = \sum_{M}\exp\left(\mathrm{i}M\omega t + \frac{1}{2}M^T DM\right),$$

$$F(\zeta) = \sum_{M}\left(\exp M^T OM - 1\right)\exp\left(\mathrm{i}M\omega\zeta + \frac{1}{2}M^T DM\right).$$

Consider now the linear part of the solution only. The function $G(\zeta)$can be written in the product form $G(\zeta) = \prod_{k=1}^{n} G_k(\zeta)$, where is the classical theta function given by the series [Magnus *et al.* (1966)]

$$G_k(\zeta) = \sum_{M_k=-\infty}^{\infty}\exp\left(\mathrm{i}M_k\omega k_n\zeta + \frac{1}{2}M_k^2 D_{kk}\right).$$

Consequently, we obtain for the linear part of the solution

$$u_{\mathrm{lin}} = \sum_{k=0}^{n} u_{k\mathrm{lin}}, \quad u_{k\mathrm{lin}} = 2\frac{\mathrm{d}^2}{\mathrm{d}\zeta^2}\log G_k(\zeta), \tag{3.8}$$

$$u_{\mathrm{lin}} = \sum_{l=1}^{n}\alpha_l\left[\frac{2\pi}{K_l\sqrt{m_l}}\sum_{k=0}^{\infty}\left(\frac{q_l^{k+1/2}}{1+q_l^{2k+1}}\cos(2k+1)\frac{\pi\omega_l\zeta}{2K_l}\right)^2\right],$$

where we recognize the linear expression (3.2) [Abramowitz and Stegun (1984)] with $K'(m_1) = K(m)$, $m+m_1 = 1$, $K = K(m) + \int_0^{\pi/2}\frac{\mathrm{d}u}{\sqrt{1-m\sin^2 u}}$.

The nonlinear term of the solution can be written in the form

$$2\frac{\mathrm{d}^2}{\mathrm{d}\zeta^2}\log\left(1+\frac{F(\zeta)}{G(\zeta)}\right)\equiv\frac{\sum\limits_{k=0}^{n}\beta_k\mathrm{cn}^2(\omega_k\zeta;m_k)}{1+\sum\limits_{k=0}^{n}\gamma_k\mathrm{cn}^2(\omega_k\zeta;m_k)}, \tag{3.9}$$

with $0\leq m_k\leq 1$. For$m_k=0$ and $m_k=1$, Eq. (3.9) is satisfied. A numerical verification of Eq. (3.9) was performed for different values of with a maximum error of 5×10^{-7}.

4 Results for the spherical nanoindentation

Recent studies [Ouyang *et al*. (2008)] have shown that for a spherical indentation in a homogeneous material, the indentation size effect depends on the indenter radius rather than penetration depth. In order to investigate these effects, we carried our analyses of indentation with indenters of different radii, as well as different penetration depth.

The comparison of our simulations against experiments is not the focus of the present paper. Our intention is to explain via Toupin-Mindlin theory the well-known size effect regarding hardness versus depth and hardness versus indenter radius in nanoindentation experiments. Therefore, we will discuss the results with experimental results if available or earlier similar results obtained by theories different from that presented here.

Let us consider the following values of the material parameters $\lambda=1.42$TPa, $\mu=2.31$TPa, $\xi_1=0.5\text{TPa}\cdot\text{m}^{-2}$, $\xi_j=0.1\text{TPa}\cdot\text{m}^{-2}$, $j=2,...,5$.

We consider three values for l= 0.5, 1 and 1.5μm, and l/R =0.1, 0.04 and 0.008, where l denotes an internal length scale which appears in Eq. (2.7). These cases corresponds to the indenter radii R =5, 10 and 15μm, R =12.5, 25 and 37.5μm, and R =62.5, 125 and 187.5μm, respectively.

Fig.3 presents the dimensionless hardness ($\bar{H}=H/H_0$) with H_0 =1TPa, versus the dimensionless indentation depth ($\bar{h}=h/h_0$) with h_0 =1nm, for l/R =0.1. The baseline corresponds to no gradient effects. The hardness $\bar{H}$ increases up to $\bar{h}=8$ (corresponding to P =2.18μm) and after that we observe a falling hardness with respect to increasing indentation depth ($\bar{h}>8$), above the baseline case with no gradient effects. The effect is weaker for smaller indenter radii.

The profile of the curve presented in Fig.3 is similar to those obtained by Lele and Anand in 2009, by applying a theory of strain-gradient viscoplasticity with finite deformations for isotropic materials. Another model with a similar profile of the curve is based on a micromechanical model that assesses a nonlinear cou-

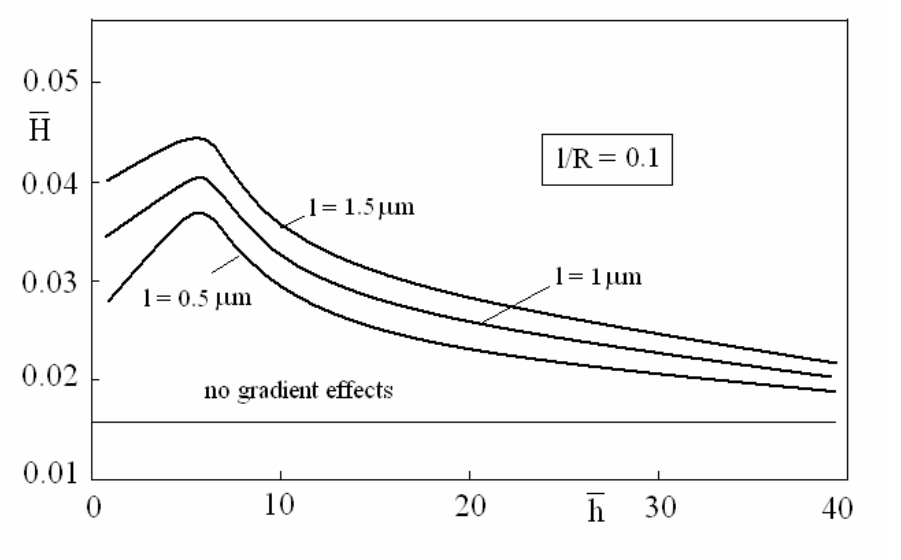

Figure 5: The hardness versus various indentation depths in the case l/R =0.1.

pling between the statistically stored dislocations and the geometrically necessary dislocations [Abu Al-Rub 2007].

While our theory of nanoindentation remains in the elastic range, the aforementioned theories' attempt is to capture the micro and nano-indentation size effect via the dependency on plastic strain gradients.

Plots of the ratios of the hardness H and the generalized stress components σ^*_{rr}, $\sigma^*_{r\varphi}$ and $\sigma^*_{r\theta}$, respectively as functions of a/R and l/R =0.1, 0.04 and 0.008, are presented in Fig.4. Similarly, the plots of ratios of the hardness H and the generalized stress components $\sigma^*_{\theta\theta}$ and $\sigma^*_{\varphi\varphi}$, respectively as functions of a/R and l/R =0.1, 0.04 and 0.008, are presented in Fig.5.

Fig. 6 presents the dimensionless hardness $\bar{H}$ with H_0 =1TPa, versus the dimensionless indentation depth ($\bar{h} = h/h_0$) with h_0 = 1nm, for l/R =0.008. The baseline corresponds to no gradient effects. The hardness $\bar{H}$ gradually slows up for $\bar{h} \leq 8$ and rapidly increases with respect to increasing $8 < \bar{h} < 30$. For $\bar{h}$ >30, the increase in $\bar{H}$ becomes less sensitive to $\bar{h}$. This type of behavior is similar to those obtained by Ouyang *et al.* (2008).

The Toupin-Mindlin theory is evaluated in order to predict and explain this peculiar behavior. The decrease or increase in $\bar{H}$ is believed to be closely associated with the loading P and the inner walls size in multiwalled nanotubes.

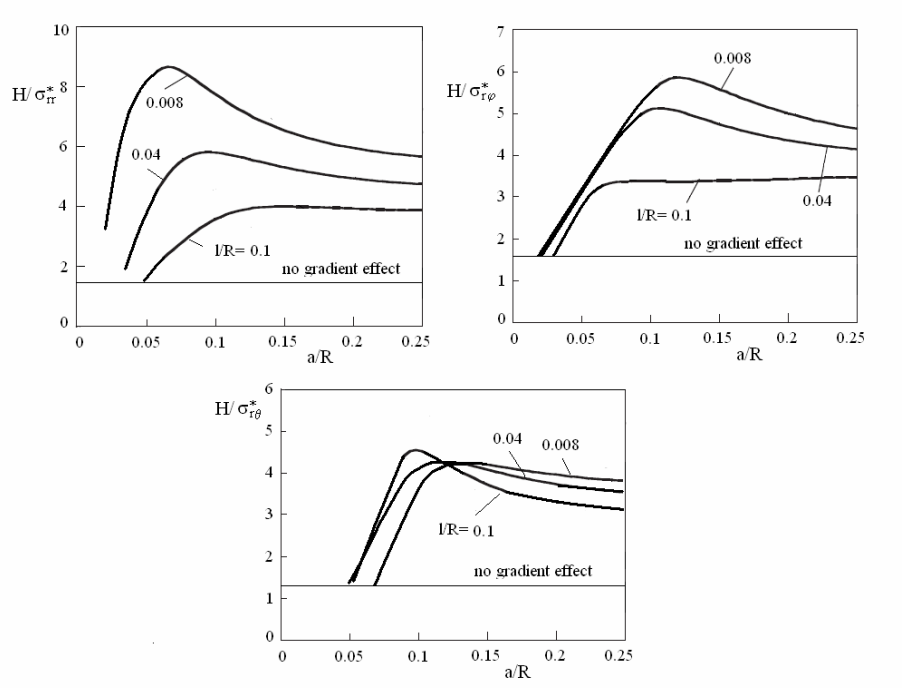

Figure 6: Ratios between the hardness H and σ^*_{rr}, $\sigma^*_{r\varphi}$ and $\sigma^*_{r\theta}$ as functions of a/R.

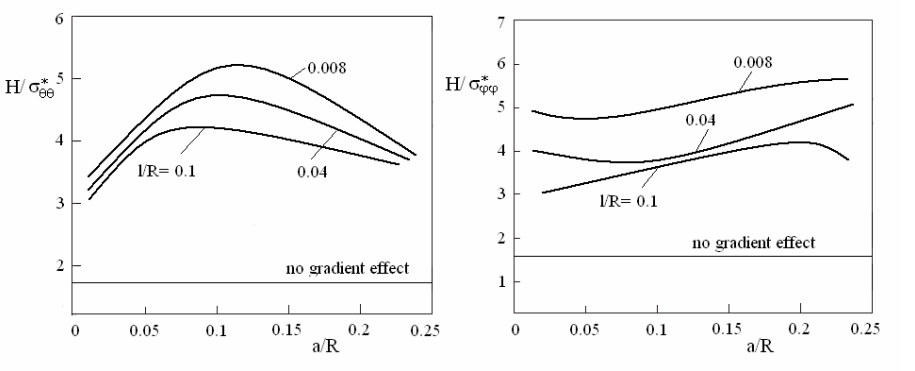

Figure 7: Ratios between the hardness H and $\sigma^*_{\theta\theta}$ and $\sigma^*_{\varphi\varphi}$ as functions of a/R.

When the dimensions of the indenter radius are comparable to the intershell walls size (fig.3), the indenter motion is easier for $P > 2.18\mu$m, and difficult for$P < 2.18\mu$m. In the first case, the hardness is decreasing with respect to the indentation depth, while in the second case, the effect is reversed.

When the dimensions of the indenter radius are larger than the intershell size (fig.6), the walls are impenetrable and the indenter motion is difficult. This leads to a strain hardening of the material, and the hardness is increasing with respect to the indentation depth. For $P < 2.18\mu$m the increase is slowly but becomes rapidly for $P > 2.18\mu$m.

By comparing Figs.3 and 6, we see that the hardness increases significantly with respect to decreasing of the indenter size. For $P > 2.18\mu$m, the intershell of the nanotubes come into contact with the indenter tip and the increase in load has different actions depending on the indenter size.

The indenter penetrability into material depends on the shear resistance of the intershell walls during the buckling of the multiwalled nanotubes. The shear resistance is calculated by taking into account the higher-order stresses gradient contribution, the latter is plotted in Fig.7. The value of the shear resistance is smaller for indenter radii $5\mu\text{m} \leq R \leq 15\mu$m than for larger indenter radii $62.5\mu\text{m} \leq R \leq 187.5\mu$m. The resistance keeps a constant value for $R > 120$. This can explain the tendency of the hardness to decrease with respect to the indentation depth for lower shear resistance, and to increase for larger shear resistance. However, it should be noted that the higher-order stresses τ_{ijk} play an important role in refining the elastic buckling theory that account for additional physics. The results presented in this study show that the size significantly affects the nanoindentation hardness.

5 Concluding remarks

It is well-known that the nanoindentation hardness displays strong indentation size effects. In this paper, the size dependence of the hardness with respect to the depth and the indenter radius for the buckling of multiwalled carbon nanotubes is investigated using the Toupin-Mindlin strain gradient theory. As expected, the indentation hardness is closely related to the depth and the indenter radius. Qualitatively, the responses of the axially compressed multiple walled carbon nanotube agree remarkable well with the experimental observations.

The tendency of the hardness to decrease with respect to the indentation depth for lower shear resistance, and to increase for larger shear resistance, is a peculiar behavior which reveals the indentation size effects. When the dimensions of the indenter radius are comparable to the intershell size, the indenter motion is easier for $P > 2.18\mu$m, and difficult for $P < 2.18\mu$m. In the first case, the hardness

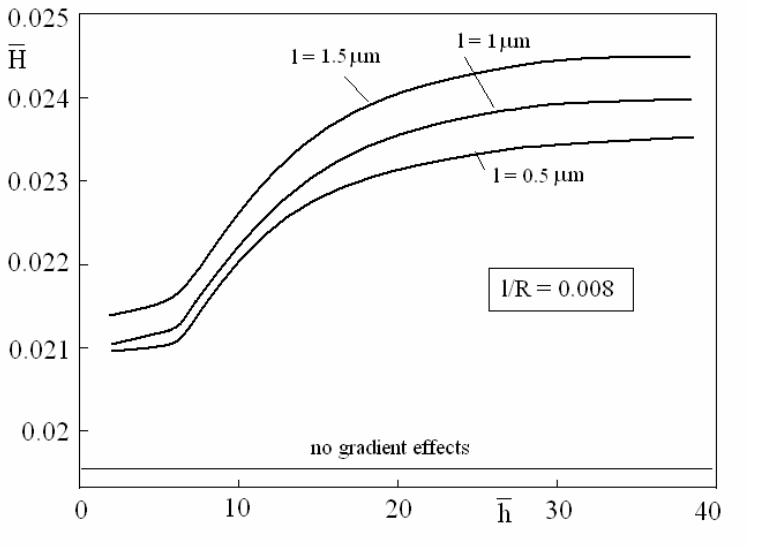

Figure 8: The hardness versus indentation depth in the casel/R =0.008.

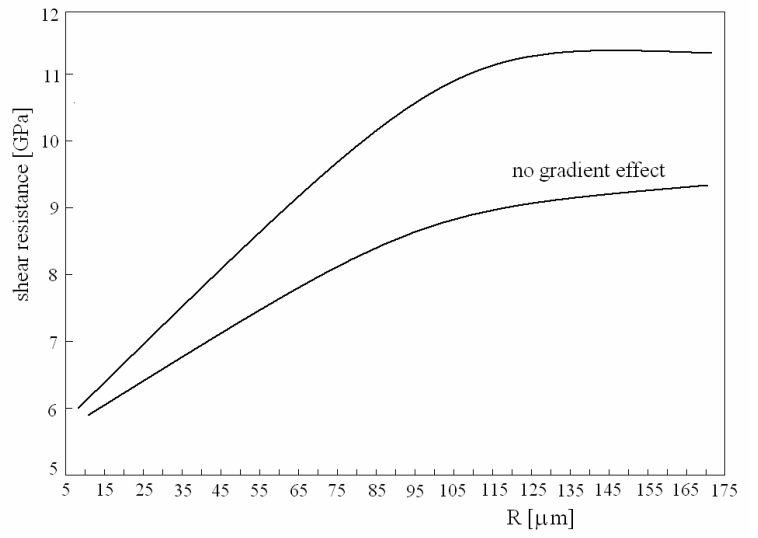

Figure 9: Shear resistance between the neighboring walls of the multiwalled nanotubes.

is decreasing with respect to the indentation depth, while in the second case, the effect is reversed. When the dimensions of the indenter radius are larger than the intershell size, the walls are impenetrable and the indenter motion becomes difficult. Therefore, the hardness is increasing with respect to the indentation depth; for $P < 2.18\mu$m the increase is slowly but becomes rapidly for $P > 2.18\mu$m. The double stresses τ_{ijk} play an important role in refining the elastic buckling theory that account for additional physics.

Acknowledgement: This research was financially supported by the National Authority for Scientific Research (ANCS, UEFISCSU), Romania, through PN2 project 106/2007, CNCSIS code 247/2007. The authors would like to extend sincere thanks to Dr. Liviu Marin for his help in preparing this paper.

References

Abramowitz, M.; Stegun, I.A. (eds.) (1984): *Handbook of mathematical functions*, U.S. Dept. of Commerce.

Abu Al-Rub, R.K. (2007): Prediction of micro and nanoindentation size effect from conical or pyramidal indentation, *Mechanics of Materials* **39**: 787–802.

Atluri, S.N.; Han, Z.D.; Shen,S. (2003): Meshless local Petrov-Galerkin (MLPG) Approaches for Solving the Weakly-Singular Traction{&) Displacement Boundary Integral Equations. *CMES: Computer Modeling in Engineering & Sciences*. **4**(5):507–518.

Atluri, S.N.; Shen, S.P. (2002a): The mesh local Petrov-Galerkin (MLPG) method: a simple & less-costly alternative to the finite element and boundary element methods. *CMES: Computer Modeling in Engineering and Sciences* **3**: 11–51.

Atluri, S.N.; Shen, S.P. (2002b): *The meshless local Petrov-Galerkin (MLPG) method*. Tech. Science Press.

Atluri, S.N.; Zhu, T. (1998): A new meshless local Petrov-Galerkin (MLPG) approach in computational mechanics. *Comput. Mech*. **22**: 117–127.

Brenner, D. W.; Shenderova, O. A.; Areshkin, D. A.; Schall, J. D.; Frankland, S.J.V. (2002): Atomic modeling of carbon-based nanostructures as a tool for developing new materials and technologies. *CMES: Computer Modeling in Engineering & Science* **3**(5): 643–673.

Bulychev, S.I.; Alekhin, V.P.; Shorshorov, M.Kh.; Ternovskii, A.P. (1976): Mechanical properties of materials studied from kinetic diagrams of load versus depth of impression during microimpression. *Strength Mater*. **8**: 1084–1089.

Bulychev, S.I.; Alekhin, V.P.; Shorshorov, M.Kh.; Ternovskii, A.P.; Shnyrev,

G.D. (1975): Determining Young's modulus from the indenter penetration diagram. *Zavod Lab.* **41.**

Chakrabarty, A.; Cagin, T. (2008): Computational studies on mechanical and thermal properties of carbon nanotube based nanostructures. *CMC: Computers Materials & Continua* **7**(3): 167–189.

Chambon, R.; Caillerie, D.; Tamagnini, C. (2004): A strain space gradient plasticity theory for finite strain. *Comput. Methods Appl. Mech. Eng*. **193**: 2797–2826.

Chambon, R.; Caillerie, D.; Matsuchima, T. (2001): Plastic continuum with microstructure, local second gradient theories for geomaterials: localization studies, *Int. J. Solids Struct*. **38**: 8503–8527.

Chambon, R.; Caillerie, D. ; El Hassan, N. (1998): One-dimensional localisation studied with a second grade model, *Eur. J. Mech.-A/Solids* **17**(4): 637–656.

Chambon, R.; Caillerie, D. ; El Hassan, N. (1996): Etude de la localisation unidimensionnelle ál'aide d'un modéle de second gradient. *C.R.A.S-Série II B* **323**: 231–238.

Chen, W.H.; Cheng, H.C.; Hsu, Y.C. (2007): Mechanical Properties of Carbon Nanotubes Using Molecular Dynamics Simulations with the Inlayer van der Waals Interactions. *CMES: Computer Modeling in Engineering & Sciences* **20**(2): 123–145.

Cheng, H.C.; Hsu, Y.C.; **Chen, W.H.** (2009): The Influence of Structural Defect on Mechanical Properties and Fracture Behaviors of Carbon Nanotubes. *CMC: Computers, Materials and Continua.* 11(2): 127–146.

Chiroiu, V.; Munteanu. L.; Donescu, St. (2006): On the mechanical modeling of single-walled carbon nanotubes. *Rev. Roum. Sci,. Techn., serie Mécanique Appl*. **51**(1): 37–52.

Collin, J.M.; Mauvoisin, G.; Abdi, R.EI. (2008): An experimental method to determine the contact radius changes during a spherical instrumented indentation. *Mechanics of Materials* **40**: 401–406.

Data E.; Tanaka, I. (1976): Periodic multi-soliton solutions of Korteweg-de Vries equation and Toda lattice, *Supplement of the Progress of theoretical Physics* **59**: 107–125.

Dubrovin B.A.; Matveev V.B.; Novikov S.P. (1976): Nonlinear equations of Korteweg-de Vries type, finite zone linear operators, and Abelian varietes, Russ. Math. Surv. 31(1): 59–146.

Dumitriu, D.; Chiroiu, V. (2008): On the modeling of nanocontacts. *Rev. Roum. Sci,. Techn., Serie MÉcanique Appl*. **53**(3).

Dumitriu, D; Gauchs, G.; Chiroiu, V. (2008): Optimisation procedure for pa-

rameter identification in inelastic material indentation testing. *Rev. Roum. Sci,. Techn., Serie Mécanique Appl*. **53**(1): 43–54.

Dumitriu, D.; Chiroiu, V. (2006): On the dual equations in contact elasticity. *Rev. Roum. Sci,. Techn., Serie Mécanique Appl*. **51**(3): 261–272.

Eringen, A.C. (1967): *Mechanics of Continua*, John Wiley & Sons, Inc.

Eshel, N.N.; Rosenfeld, G. (1975): Axi-symmetric problems in elastic materials of grade two. *J. Franklin Inst*. 299, 43–51.

Eshel, N.N.; Rosenfeld, G. (1970): Effects of strain-gradient on the stress-concentration at a cylindrical hole in a field of uniaxial tension. *J. Eng. Math*. 4, 97–111.

Evans, A.G., Hutchinson, J.W. (2009): A critical assessment of theories of strain gradient plasticity. *Acta Materialia*, **57:** 1675–1688.

Fleck, N.A.; Hutchinson, J.W. (2001): A reformulation of strain gradient plasticity. *J. Mech. Phys. Solids* 49: 2245–2271.

Fleck, N.A.; Hutchinson, J.W. (1997): *Strain gradient plasticity*. In: Hutchinson, J.W., Wu, T.Y. (Eds.), In: Adv. Appl. Mech., vol. 33. Academic Press, New York, 295–361.

Fleck, N.A.; Hutchinson, J.W. (1993): A phenomenological theory for strain gradient effects in plasticity. *J. Mech. Phys. Solids* **41**(12): 1825–1857.

Galin, L.A. (1946): Spatial contact problems of the theory of elasticity for punches of circular shape in planar projection. *J. Appl. Math. Mech*. (PMM) **10**: 425–448.

Georgiadis, H.G.; Grentzelou, C.G. (2006): Energy theorems and the J-integral in dipolar gradient elasticity. *Int. J. Solids Struct*. **43**: 5690–5712.

Giannopoulos, G.I.; Georgantzinos, S.K.; Katsareas, D.E.; Anifantis, N.K. (2010): Numerical prediction of Young's and shear moduli of carbon nanotube composites Incorporating Nanosxcale and interfacial effects. *CMES: Computer Modeling in Engineering & Sciences* 56(3): 231–248.

Ghanbari, J.; Naghdabadi, R. (2009): Multiscale nonlinbear constitutive modeling of carbon nanstructures based on interatomic potentials. *CMC: Computers, Materials and Continua.* 10 (1): 41–64.

Gumbsch, P. (1996): An atomistic study of brittle fracture: toward explicit failure criteria from atomistic modeling. *Journal of Material Resource* **10**: 2897–2907.

Han, Z.D.; Atluri, S.N. (2003): Truly Meshless Local Patrov-Galerkin (MLPG) solutions of traction & displacement BIEs. *CMES: Computer Modeling in Engineering & Sciences*, **4**(6): 665–678.

Hay, J.C.; Wolff, P.J. (2001): Small correction required when applying the Hertzian contact model to instrumented indentation data. *J. Mater. Res*. **16**(5): 1280–1286.

Hernot, X.; Bartier, O.; Berkouche, Y.; El Abdi, R.; Mauvoisin, G. (2006): Influence of penetration depth and mechanical properties on contact radius determination for spherical indentation. *Int. J. Solids Struct.* **43**(14-15): 4136–4153.

Hiroshi Kadowaki; Liu Wing Kam (2005): A multiscale approach for the micropolar continuum model, *CMES: Computer Modeling in Engineering & Sciences*, 7(3): 269–282.

Hutchinson, J.W. (2000): Plasticity at the micron scale. *Int J Solids Structures* **37**: 225–238.

Jeng, Y-R.; Tsai, P-C.; Huang, G-Z. ; Chang, I-L. (2009): An Investigation into the mechanical Behavior of Single-Walled Carbon Nanotubes under Uniaxial Tension Using Molecular Statics and Molecular Dynamics Simulations. *CMC: Computers, Materials and Continua* **11**(2): 109–125.

Johnson, K.L. (1985*): Contact Mechanics,* Cambridge University Press, New York.

Kaczmarczyk, L. (2006): Enforcing boundary conditions in micro-macro transition for second order continuum. *CMC: Computers, Materials and Continua* **4**(2): 55–62.

Keerthika, B.; Cao, Y.P.; Raabe, D. (2009): Mechanical Characterization of Viscoelastic-Plastic Soft Matter Using Spherical Indentation. *CMC: Computers, Materials and Continua.* **10**(3): 243–258.

Kikuchi, M.; Miyamoto, H.; Atluri, S.N. (1985): Studies on Size Effects and Crack Growth of Side-Grooved Specimens. *Fracture Mechanics: Sixteenth Symposium*, ASTM/STP 868, M.F. Kanninen and A.T. Hooper, Eds., Philadelphia: 251–278.

Lele, S.P.; Anand, L. (2009): A large-deformation strain-gradient theory for isotropic viscoplastic materials. *International Journal of Plasticity* **25**: 420–453.

Li, K.; Wu, T.W.; Li, J.C.M. (1997): Contact area evolution during an indentation process. *J. Mater. Res*. 12 (8): 2064–2071.

Li, C.Y.; Chou T.W. (2003): Elastic moduli of multi-walled carbon nanotubes and the effect of van der Waals forces. *Composites Science and Technology*. **63**: 1517–1524.

Li, Q.; Shen, S., Han, Z.D.; Atluri, S.N. (2003): Application of the Meshless Local Petrov-Galerkin (MLPG) Method to Problems with Singularities, and Material Discontinuities, in 3-D Elasticity, *CMES: Computer Modeling in Engineering & Sciences*. **4** (5):571–586.

Ma, Q.; Clarke, D.R. (1995): Size dependent hardness of silver single crystals. *J. Mater. Res*. 10: 853–863.

Magnus W.; Oberhettinger R.; Soni P. (1966): *Formulas and Theorems for the Special Functions of Mathematical Physics,* Springer, New York.

Mindlin, R.D.; Eshel, N.N. (1968): On first strain-gradient theories in linear elasticity. *Int. J. Solids Struct*. **4**: 109–124.

Mindlin, R.D. (1965): Second gradient of strain and surface tension in linear elasticity. *Int. J. Solids Struct*. **28**: 845–857.

Mindlin, R.D. (1964): Micro-structure in linear elasticity. *Arch. Ration. Mech. Anal*. **16**: 51–78.

Misra, A.; Huang, S. (2009): Micromechanics based stress-displacement relationships of rough contacts: Numerical implementation under combined normal and shear loading. *CMES: Computer Modeling in Engineering & Sciences* **52**(2): 197–216.

Munteanu, L.; Chiroiu, V. (2010): On the locally resonant sonic composites' dynamics. *EUROPEAN JOURNAL OF MECHANICS-A/SOLIDS* (IN PRESS).

Munteanu, L.; Chiroiu, V. (2009): Shell Buckling of Carbon Nanotubes Using Nanoindentation. *CMES: Computer Modeling in Engineering & Science* **48** (1): 27–41.

Munteanu, L.; Donescu, St. (2004): *Introduction to Soliton Theory: Applications to Mechanics,* Book Series "Fundamental Theories of Physics", 143, Kluwer Academic Publishers.

Nair, A.K.; Farkas, D.; Kriz, R.D. (2008): Molecular Dynamics Study of Size Effects and Deformation due to Nanoindentation. *CMES: Computer Modeling in Engineering & Sciences* 24(3): 239–248.

Nasdala L.; Ernst G.; Lengnick M.; Rothert H. (2005): Finite Element Analysis of Carbon Nanotubes with Stone-Wales Defects, *CMES: Computer Modeling in Engineering & Sciences*, **7**(3): 293–304.

Oliver, W.C.; Pharr, G.M. (1992): Improved technique for determining hardness and elastic modulus using load and displacement sensing indentation experiments. *Journal of Materials Research* **7**(6): 1564–1580.

Osborne, A.R. (1995): Soliton physics and the periodic inverse scattering transform. *Physica D* **86**: 81–89.

Ouyang, C.; Li, Z.; Huang, M.; Hou, C. (2008): Discrete dislocation analyses of virvular nanoindenttaion and its size dependence in polycrystals. *Acta Materialia* **56**: 2706-2717.

Qian, X.; Cao, Y.; Zhang, J.; Raabe, D.; Yao, Z.; Fei, B. (2008): An Inverse Approach to determine the mechanical properties of Elastoplastic Materials Using Indentation Tests.*CMC: Computers, Materials and Continua*. **7**(1): 33–41.

Rino, J.P.; Cardozo, G.O.; Picinin, A. (2009): Atomistic Modeling of the Strcutural and Thermal Conductivity of the InSb. *CMC: Computers, Materials and Continua.* **12**(2): 145–156.

Ru, C.Q. (2001): Axially compressed buckling of a doublewalled carbon nanotube embedded in an elastic medium. *Journal of Mechanics and Physical Solids*, **49**: 1265–1279.

Shen, S.; Atluri, S.N. (2004): Computational Nano-mechanics and Multi-scale Simulation, *CMC: Computers, Materials, & Continua.* **1**(1), 59–90.

Shorshorov, M.Kh., Bulychev, S.I., Alekhin, V.P. (1981): Work of plastic and elastic deformation during indentation. *Sov. Phys. Dokl*. **26**: 769–771.

Sneddon, I.N. (1965): The relation between load and penetration in the axisymmetric Boussinesq problem for a punch of arbitrary profile. *Int. J. Eng. Sci*. **3**.

Solano C.J.F.; Costales A.; Francisco E.; Pendáas A.M.; Blanco M.A.; Lau K.C.; He H., Pandey R. (2008): Buckling in Wurtzite-Like AIN Nanostructures and Crystals: Why Nano can be Different. *CMES: Computer Modeling in Engineering & Sciences* 24(2): 143–156.

Srivastava, D.; Atluri, S.N. (2002): Computational Nano-technology: A Current Perspective. *CMES: Computer Modeling in Engineering & Sciences* 3(5): 531–538.

Tabor, D. (1951): *The Hardness of Metals.* Clarendon Press, Oxford, UK.

Tang, Z.; Shen, S.; Atluri, S.N. (2003): Analysis of materials with strain gradient effects: A Meshless local Petrov-Galerkin approach, with nodal displacements only. *CMES: Computer Modeling in Engineering & Sciences* 4(1): 177-196.

Theodosiou, T.C.; Saravanos, D.A. (2007): Molecular Mechanics Based Finite Element For Carbon Nanotube Modeling. *CMES: Computer Modeling in Engineering & Sciences* 19(2): 121–134.

Toupin, R.A. (1964): Theories of elasticity with couple-stress. *Arch. Ration. Mech. Anal*. **17** (2): 85–112.

Toupin, R.A. (1962): Elastic materials with couple stresses. *Arch. Ration. Mech. Anal*. **11**: 385–414.

Volokh, K.Y. (2006): Lagrangian equilibrium equations in cylindrical and spherical coordinates. *CMC: Computers, Materials and Continua.* **3**(1): 37–42.

Waters, J.F.; Guduru, P.R.; Jouzi, M.; Xu, J.M. (2005): Shell buckling of individual multiwalles carbon nanotubes using nanoindentation. *Applied Physics Letters* **87**: 103–109.

Xie, G.Q.; Han, X.; Long, S.Y. (2007): Characteristic of waves in a multi-walled

carbon nanotube. *CMC: Computers, Materials and Continua*. **6**(1): 1–12.

Xie, G.Q.; Long, S.Y. (2006): Elastic Vibration Behaviors of Carbon Nanotubes based on Micropolar Mechanics. *CMC: Computers, Materials and Continua*. **4**(1): 11–19.

Zhao, J.; Pedroso, D (2008): Strain gradient theory in orthogonal curvilinear coordinates. *Int. J. Solids Struct.* **45**: 3507–3520.

Zhao, J.D.; Sheng, D.C.; Sloan, S.W.; Krabbenhoft, K. (2007a): Limit theorems for gradient-dependent elastoplastic geomaterials, *Int. J. Solids Struct*. **44**: 480–506.

Zhao, J.D.; Sheng, D.C.; Sloan, S.W. (2007b): Cavity expansion of a gradient-dependent solid cylinder. *Int. J. Solids Struct.* 44: 4342–4368.

Zhao, J.D., Sheng, D.C. (2006): Strain gradient plasticity by internal-variable approach with normality structure. *Int. J. Solids Struct*. 43: 5836–5850.

Zhao, J.D.; Sheng, D.C.; Collins, I.F. (2006): Thermomechanical formulation of strain gradient plasticity for geomaterials. *J. Mech. Mater. Struct*. 1(5): 837–863.

Zhao, J.D.; Sheng, D.C.; Zhou, W.Y. (2005): Shear banding analysis of geomaterials by strain gradient enhanced damage model. *Int. J. Solids Struct*. 42 (20): 5335–5355.